Archives of Hydro-Engineering and Environmental Mechanics
Vol. 54 (2007), No. 1, pp. 55–73

Measurements of 3D Turbulence Structure in a Compound Channel

Włodzimierz Czernuszenko[*], Adam Kozioł[**], Paweł M. Rowiński[*]

[*]Institute of Geophysics, Polish Academy of Sciences, Ks. Janusza 64, 01-452 Warsaw, Poland,
emails: wczer@igf.edu.pl, adam_koziol@sggw.pl, pawelr@igf.edu.pl
[**]Warsaw Agricultural University SGGW, ul. Nowoursynowska 159, 02-776 Warsaw, Poland

(Received February 23, 2007; revised March 20, 2007)

Abstract

The paper describes some turbulence measurements carried out in an experimental compound channel with flood plains. The surface of the main channel bed was smooth and made of concrete, whereas the floodplains and sloping banks were covered by cement mortar composed with terrazzo. Instantaneous velocities were measured be means of a three-component acoustic Doppler velocity meter (ADV) manufactured by Sontek Inc. This article presents the results of measurements of primary velocity, the distribution of turbulent intensities, Reynolds stresses, autocorrelation functions, turbulent scales, as well as the energy spectra.

Key words: open channel, compound channel, turbulence, measurements

1. Introduction

An important feature of most rivers in their midstream or downstream reach is a compound cross-section, consisting of a deep main channel, usually with inclined banks, and shallow floodplains, which are often rough due to vegetation. In these channels flood conditions lead to a complex, 3D flow situation with intensive mass and momentum exchange between the main channel and the floodplains. This produces a transverse shear layer influencing the flow in both the main channel and the floodplains. The momentum transfer takes place not only by the bed generated turbulence, but also by free shear turbulence and secondary currents. It is now well established that the proper evaluation of this so-called "interaction mechanism" is crucial for reliable prediction of the flow field and related processes, such as flooding, spreading of pollutants, and transport of solids due to sedimentation and erosion. The structure of turbulence in such flows is extremely complex. To investigate this structure many experimental works have been performed (see e.g. Knight, Shiono 1990, 1996, Arnold 1989, Knight et al 1994, Shiono, Knight 1990, 1991, Rhodes and Knight 1994, Tominaga et al 1989).

The application of mathematical turbulence models for predicting the 3D flow in compound channels requires high quality data for validation purposes. All mathematical turbulence models introduce a number of empirical constants to describe Reynolds stresses, eddy viscosity, mixing length and other parameters (Naot and Nezu 1993, Nezu at al 1999, Czernuszenko and Rylov 2002, Prooijen and Uijttewaal 2005). To determine all these parameters, specially designed experimental works are greatly needed. In some papers the problem of developing a good conceptual model of the interaction between the main channel and floodplain is considered. One dominant feature, are the vortices with vertical axes which develop in any highly sheared zone between two co-flowing streams at different velocities. These vortices are responsible for convecting high momentum fluid from the main channel onto the floodplain. The second feature is the longitudinal vorticity causing perturbations in any lateral distribution of boundary shear stress. Also, secondary flows are the reason for distraction of the distribution of the stresses. Secondary flows are usually directed inwards to channel corners and outwards at re-entrance corners. All these features indicate the three dimensional nature of all the vorticies and also the complexity of the turbulence in the interaction zone. Since they are still not yet fully understood, reliable measurements are very important and needed.

There are also other issues calling for special attention. One of them is the logarithmic velocity law, which is not necessarily valid in the complex region where the interaction process between the river and its floodplain is most intense. One would expect the logarithmic velocity distribution at the channel centerline where the flow is essentially two-dimensional. At other locations, notably near the corner region in trapezoidal channels and at the main channel/floodplains interface in overbank flow, the flow is clearly 3D in nature and deviations from logarithmic law are expected. Also, the vertical and lateral distributions of Reynolds stresses in the compound channel are the main issues to consider and a very important question arises. It is of crucial importance whether the vertical distribution of the Reynolds stress term τ_{zx} is linear or not. It is well known, that the positive answer to this question is only in the case of 2D flow. Then, the vertical distribution is approximately linear at the centerline of the channel, but not in the vicinity of the main river bank. Also, it is interesting to know how the Reynolds stress term τ_{yx} is distributed in the lateral direction. It is obvious, that at the channel centerline this stress should become trivial.

The scope of this paper is to provide results of comprehensive measurements of main turbulence parameters in steady turbulent flow in a trapezoidal straight channel with the symmetrical, complex cross-section with inclined side-walls. It is a continuation and an extension of the study published in Rowiński et al (2002) in which a similar experimental program, with use of 1D velocity meter, was fulfilled. This time the full three-dimensional velocity field is under consideration due to the use of 3D Acoustic Doppler Velocity (ADV) meter. The case with a smooth main channel and rough floodplains is considered in the study. A separate measuring

campaign with vegetated floodplains has been analyzed in Rowiński and Mazurczyk (2006).

2. Theoretical Considerations

In principle, a detailed description of the flow structure in a compound channel requires three-dimensional analyses, but the classical theory of the two-dimensional mean flows using the statistical theory of turbulence, remains a fundamental base allowing to obtain approximate results explaining basic phenomena. The two-dimensional, steady and uniform turbulent flow in an open channel is governed by the Reynolds-averaged Navier-Stokes equations. The equation for the longitudinal streamwise component of momentum of a fluid element may be combined with the continuity equation to give (Shiono and Knight 1991):

$$\frac{\partial UV}{\partial y} + \frac{\partial UW}{\partial z} = g \sin\theta + \frac{1}{\rho}\left(\frac{\partial \tau_{yx}}{\partial y} + \frac{\partial \tau_{zx}}{\partial z}\right), \tag{1}$$

where x, y, z are streamwise, lateral and normal directions respectively; U, V, W are temporal mean velocity components; ρ is the density of water, θ is the bed slope, g is the gravitational acceleration, τ_{ij} is the shear stress in the j-th direction ($j = x$) on the plane perpendicular to the i-th direction ($i = y$ or $i = z$). Further in the paper quantities u, v, w appear and they denote turbulent velocity components corresponding to x, y and z.

To define the vertical distribution of the local shear stress on any horizontal plane in the x-direction, Eq. (1) should be integrated from any point z above the channel bed to the water surface assuming $W = 0$ and $\tau_{zx} = 0$ at $z = h$. It gives

$$\tau_{zx} = \rho g(h - z)\sin\theta + \int_z^h \frac{\partial \tau_{yx}}{\partial y} dz - \int_z^h \frac{\partial \rho UV}{\partial y} dz + \rho UW. \tag{2}$$

The distribution of τ_{zx} is linear over the depth, only in the absence of lateral shear and secondary flows, i.e. τ_{zx} varies from 0 to $\rho g h \sin\theta$ as z varies from h to 0 (from the free surface towards the channel bed). That linear shear stress distribution together with Prandtl's model lead to the well-known logarithmic velocity distribution law in the form:

$$\frac{U}{U_*} = \frac{1}{\kappa} \ln\frac{z}{k} + B, \text{ where } \begin{cases} k = \nu/U_*, \; B \equiv B_s = 5.5 & \text{for smooth channels} \\ k \equiv k_s, \; B \equiv B_r = 8.5 & \text{for rough channels} \end{cases} \tag{3}$$

where:

U_* – friction velocity,
κ – Karman constant,

z – distance from the wall,
ν – molecular (kinematic) viscosity,
B – universal constant and
k_s – sand roughness.

2.1. Turbulence Velocities

Turbulent flow velocity at any point is by definition a random variable. The behavior of this velocity can be described by probability density function, $p(u)$. Velocity measurements provide a time series of values recorded at time instants at regular intervals Δt. We restrict our considerations to stationary and ergodic random processes. For this situation, the probability density function (pdf) is invariant with respect to time and only one sample record over a sufficiently long time interval is needed to define the pdf and relevant statistical characteristics. Thus, all information about the turbulent velocity at a point can be obtained from one time series.

The pdf and the statistical moments in this paper depend only on the magnitudes of the velocities measured at one point in the flow and not on the sequence in which those values occur. On the contrary, relevant correlation functions and energy spectra depend on the sequence in which those magnitudes occur. Reynolds stresses depend on the simultaneously recorded velocities in two directions at a point, but similarly to the pdf function they are independent from the sequence of values.

An analytical expression for the pdf for turbulent flows is not easy to establish. Nevertheless, for most practical (engineering) purposes, the function can be characterized by statistical moments of different orders that can be obtained relatively easily from experiments. A statistical moment of n-th order for a stationary, ergodic process, for any random variable (ξ) can be defined by

$$E[\xi^n] \equiv \overline{\xi^n} = \lim_{T\to\infty} \frac{1}{T} \int_{t_0}^{t_0+T} \xi^n dt, \tag{4}$$

where $E[\ ]$ represents the expected value, ξ is the random variable, $n = 1, 2, 3, \ldots$; the overbar indicates time-averaging, $t = t_0$ at the beginning of the data series being analyzed, and T is the duration of the data time series.

The first central moment of the turbulent velocity is zero because the average turbulent velocity is zero. The second moment represents the mean-square departure from the time-averaged velocity and is called the variance (σ^2) or mean square. The second, the third and fourth moments are often replaced by their non-dimensional forms, namely

$$\frac{\sigma_x}{U_*} = \frac{\sqrt{\overline{u^2}}}{U_*}, \tag{5}$$

$$S_x = \frac{\overline{u^3}}{\left(\overline{u^2}\right)^{3/2}}, \tag{6}$$

$$K_x = \frac{\overline{u^4}}{\left(\overline{u^2}\right)^2} - 3. \tag{7}$$

These non-dimensional parameters are called relative turbulence intensity (Eq. 5), skewness or excess (S_x) and flatness factor or kurtosis (K_x). Above, for simplicity, they are defined only for the longitudinal component. These expressions have specific physical interpretations. The skewness is related to the asymmetry in the distribution of turbulent velocities. In case of a Gaussian and any other symmetrical distributions, S_x assumes zero value. S_x is positive when large positive values of instantaneous point velocities u are more frequent than large negative values. The excess is related to the flatness of the distribution. For reference, K_x = 0 for Gaussian distribution when the definition in Eq. (7) is used. Larger values of K_x imply that $p(u)$ has a narrower peak and broader tails than the Gaussian distribution with the same standard deviation. It means that both very small and very large values of the random variable are more probable than in the case of a normal distribution.

2.2. Autocorrelation Function and Energy Spectrum

Now, we may define an Eulerian autocorrelation coefficient (r_E) for the values of a given longitudinal velocity component at a fixed point in the flow field, but at two different times t and t'. Since we are working with stationary variables, r_E can depend only on the time shift τ, which is equal to $t' - t$, and it must be a symmetrical function of τ. Using Eq. (4) for time averaging, r_E for the longitudinal velocity is defined by

$$r_E(\tau) = \frac{R_E(\tau)}{\overline{u^2}}, \tag{8}$$

where $R_E(\tau) = \overline{u(t)u(t+\tau)}$.

The maximum value is $r_E(0) = 1$, while r_E approaches zero for large τ, but frequently decreasing oscillations are obtained as r_E is approaching zero. The autocorrelation coefficient can be used to define an Eulerian integral time scale (T_E) as

$$T_E = \int_0^\infty r_E(\tau)d\tau. \tag{9}$$

T_E may be considered as an indication of the time interval over which the longitudinal velocity component at a point is correlated with itself.

Let us consider a stationary and homogeneous turbulent flow with a small relative intensity. Then the hypothesis of "frozen turbulence" is valid and an integral length scale (L_x) can be calculated from the Eulerian time scale (e.g. Hinze 1975):

$$L_x = \overline{U} T_E. \tag{10}$$

The length scale defined by Eq. (10) is to a certain extent a measure of the correlation distance between the longitudinal velocities at two points of the flow field and it is called a macroscale of turbulence.

Introducing the energy or power density spectrum, we assume that the velocity fluctuation $u(t)$ can be represented by the Fourier integral. Because the auto-correlation function $R_E(t)$ of a stationary random function is an even function of t, and the power spectrum $E(f)$ and the function $R_E(t)$ are the Fourier cosine transforms, hence we may write

$$E(f) = 4 \int_0^\infty R_E(t) \cos 2\pi f t \, dt, \tag{11}$$

$$R(t) = \int_0^\infty E(f) \cos 2\pi f t \, df. \tag{12}$$

Function $E(f)$ defines the kinetic energy associated with the infinitesimal range of frequencies $(f, f + df)$. For flows in open channels, it is not a homogenous function. Its maximum values occur at the lower frequencies and the minimum one at the higher frequencies.

Kolmogoroff's similarity theory postulates that in a turbulent motion, at sufficiently high Reynolds numbers, there is a range of high frequencies where the turbulence is statistically in equilibrium and uniquely determined by the mean rate of energy dissipation per unit volume, ε, and the kinetic viscosity of the fluid, ν. This range of frequencies is called the universal, equilibrium range. If the equilibrium range is sufficiently large, it comprises a subrange (inertial subrange) where the dissipation is negligibly small compared with the flux of energy transferred by inertial effects. In such subrange the energy spectrum of turbulence can be expressed in the form which is called Kolmogoroff's spectrum law.

$$E(f) = \left(\frac{2\pi}{U}\right)^{-2/3} A \, \varepsilon^{2/3} f^{-5/3}. \tag{13}$$

3. Experimental Equipment and Methodology

The experiments were carried out in a concrete flume, 16 m long and 2.10 m wide with symmetrically complex trapezoidal cross-section. The bed slope of the channel was 0.5‰. A row of PCV pipes was installed in the initial channel reach to subside the stream. One cross-section in the middle of the flume was selected for velocity measurements (Fig. 1). It consisted of 23 verticals – six on each floodplain and eleven in the main channel.

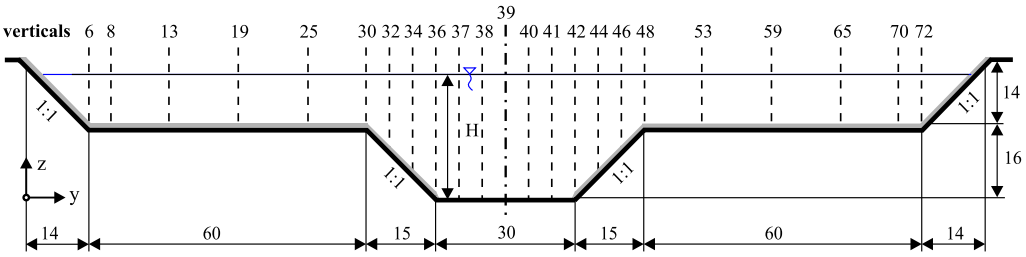

Fig. 1. Scheme of the experimental cross-section with the arrangement of measuring verticals

Water levels in the main channel and on the floodplains, all three components of point velocities, water temperature and water discharge were measured during the course of the experiment. Water depth in the channel was recorded with use of a needle level gauge. Instantaneous velocities were measured with use of a three-component acoustic Doppler velocity meter (ADV) manufactured by Sontek Inc. The acoustic sensor was mounted on a rigid stem attached to a specially designed trolley allowing for its detailed positioning. ADV works on pulse-to-pulse coherent Doppler techniques in relatively high temporal resolution (Lohrmann et al 1994). ADV proved to yield a good description of the turbulence characteristics when certain conditions related to the flow itself and the configuration of the instrument are satisfied. The measurements were conducted with maximum frequency 25 Hz in the velocity range of 0 to 1.0 m/s with the accuracy of 0.25 cm/s. Sampling volume was equal to 0.1 cm^3. Buffin-Bélanger and Roy (2005) report, that for the most turbulent statistics sufficient record length for the measurements is 60–90 s. In cases of our experiments even longer time series (120–360 s) were recorded to provide reliability of data and constancy of higher order velocity moments. Both down-looking sensor orientation and side-looking probes (close to the water surface, less than 6 cm in order to avoid flow interference) were utilized during the measurements.

Water discharges were recorded with use of a measuring circular overfall – 540 mm in diameter. During the experiment $Q = 95.20$ l/s. Water surface slope was measured by recording the pressure differences among piezometers located along the centerline of the channel bed at the distances 4 and 12 m from the channel

entrance. The surface of the main channel bed was smooth (Manning roughness coefficient $n = 0.011$ $m^{-1/3}s$) and made of concrete whereas the floodplains and sloping banks were covered by cement mortar composed with terrazzo with grains of 0.5 to 1 cm in diameter ($n = 0.018$ $m^{1/3}s$). The water depth in the main channel was kept at the level of $H = 28.3$ cm and on the floodplains $h = 12.3$ cm. The main channel width was equal to 28 cm and the floodplains' width was 60 cm. The sloping banks were inclined at the angle 1:1.

4. Analysis of Experimental Data

Mean velocity distributions in the main channel (Fig. 2; verticals 37–41) coincide with the logarithmic profile over a smooth bed with universal value of Karman constant (0.41) and constant $B = 5.5$. That good agreement is observed up to the water depth $z/h = 0.23$, e.g. to $z^+ = zU_*/\nu = 1000$. Above that value the measured velocities are larger than the ones obtained from the log-law. The increases in those values are revealed in the increase of constant B in Eq. 3. Karman value has not been treated as a priori given and it has been computed from the logarithmic profile. Log-profile allowed also for obtaining the value of shear velocity as well as the equivalent sand roughness. Bed shear stresses were obtained by extrapolation taking into account the linear distribution of Reynolds stresses. The computational results are summarized in Table 1 and Table 2.

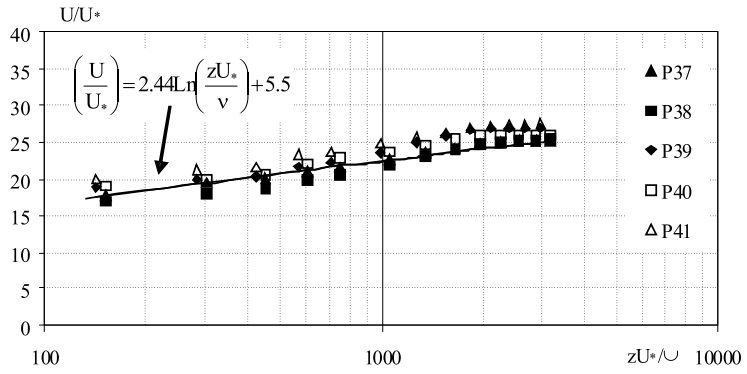

Fig. 2. Mean velocity distribution in the main channel

The mean velocity distributions are consistent with the interpretation of Eq. 2 – for negligible values of vertical and transverse velocities V and W and negligible values of transverse Reynolds stresses, the stresses τ_{zx} vary linearly with the distance from the bed which leads to logarithmic profile. As stated above, similar computations were made for the flow above the sloping banks (verticals 32, 34, 44 and 46) and it is observed that flow in that area is three-dimensional. In spite of relatively

Table 1. Karman constant, shear stress at the bed level ($\tau_{xz}/\rho = -\overline{uw}$) and shear velocities in the main channel

Verticals	37	38	39	40	41
Karman constant, κ	0.41	0.41	0.42	0.40	0.40
$-\overline{uw}$ at the bed [(m/s)^2]	2.06 10^{-4}	2.69 10^{-4}	2.79 10^{-4}	2.38 10^{-4}	2.21 10^{-4}
$(U_*)^2$ [(m/s)^2]	2.56 10^{-4}	2.56 10^{-4}	2.25 10^{-4}	2.56 10^{-4}	2.25 10^{-4}

Table 2. Karman constant κ and equivalent sand roughness on floodplains evaluated on the basis of a logarithmic profile

	Left floodplain				Right floodplain			
Verticals	13	19	25	30	48	53	59	65
Karman constant κ	0.41	0.4	0.41	0.41	0.42	0.40	0.40	0.40
equivalent sand roughness k_s [mm]	2.1	0.9	0.5	1.8	1.5	2.6	2.9	3.2

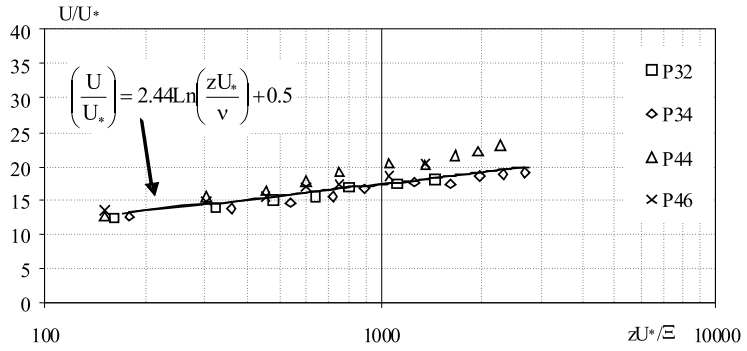

Fig. 3. Mean velocities distributions above sloping banks in the main channel

large dispersion of measuring values, they were approximated by a log-profile with Karman constant and $B = 0.5$ (Fig. 3).

In case of both floodplains a big scatter of measured values of velocities was also observed, but the values of Karman constant oscillate close to the value of 0.41 (Table 2). Since the floodplains are characterized by rough bed surface, the equivalent sand roughness was obtained taking the friction velocity from Table 1 and $B = 8.5$. It is unfortunately difficult to evaluate the value of the bed shear stress and the equivalent sand roughness in case of the flow above the terminal (left and right) sloping banks. When using similar computational technique like for the main channel, large scatter of results was observed and the only quantity assuming similar values in each case was Karman constant.

5. Higher Moments

5.1. Turbulent Intensity

Phenomenological universal functions for turbulence intensities were proposed by Nezu and Nakagawa (1993) in the form

$$\frac{\sqrt{\overline{u_i^2}}}{U_*} \equiv \frac{u_i'}{U_*} = D_i \exp\left(-C_k \frac{y}{h}\right), \tag{14}$$

where D_i and C_k are empirical constants, $i \equiv x, y, z$, and $u_1' = u'$, $u_2' = v'$, $u_3' = w'$.

Based on the best fit procedure for all points located within the range $0.1 < z/h < 0.6$, values of constants D_i and C_k in Eq. (14) at the center of the main channel (vertical 39) for all three components of velocity were obtained as $D_x = 2.29$, $D_y = 1.47$, $D_z = 1.07$. In the computations it was assumed that $C_k = 1$, as was suggested by Nezu and Nakagawa (1993), for two-dimensional flows. In fact, the values of C_k were very close to unity, especially for transverse components. In case of the verticals located a large distance from the center of the cross-section (verticals 37 and 38) the values of those coefficients are scattered. The lowest coefficients occurred at the corner between the main channel and the inclined wall (vertical 36). One can conclude, that they are attenuated by the inclined wall. For the next two verticals located over this wall these coefficients gradually increase, so that for vertical 32 these coefficients reached the maximum values of 2.94, 2.07 and 1.29, respectively (see Table 3).

Table 3. Coefficients of Eq. (1) for verticals in main channels (37–39) and for inclined wall (32–36)

	Vertical	D_u	C_k	D_v	C_k	D_w	C_k
Main channel and sloping bank	39	2.29	1	1.47	1	1.07	1
	38	2.41		1.46		1.08	
	37	2.46		1.55		1.14	
	36	1.89	0.99	1.11	0.73	0.78	0.58
	34	2.64	0.68	1.47	0.48	1.25	0.48
	32	2.94	0.28	2.07	0.90	1.29	0.22

The effect of a free surface exerted upon the turbulent intensities is easily observable for the longitudinal and lateral components starting from the relative depth $z/h = 0.68$. The values of those intensities are even larger than one could expect. The most noticeable feature is that the vertical intensities decrease rapidly towards the bottom of the channel (see Fig. 4) causing the damping of the vertical fluctuations. Probably, a similar effect occurs near the free surface, but at distances larger than $z/h > 0.75$, in the zone not registered during our measurements (Fig. 4).

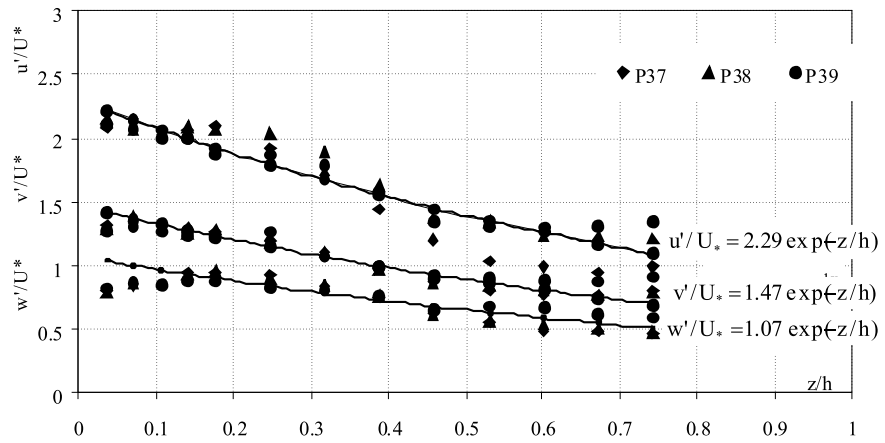

Fig. 4. Three components of turbulence intensities in the main channel (for notation see Eq. 14)

Some differences for the verticals located over the inclined wall (interaction zone) have been observed, namely for two verticals P32 and P34 for which the turbulence intensities are significantly higher than those in the main channel. This profile of the turbulence intensity is strongly influenced by the inclined wall. Coefficient D_u varies from the lowest value at the vertical 36 to the highest one at the vertical 32 for all components of the intensity. In the case of interactive zone the parameter C_k is generally less than unity (see Table 3).

5.2. Skewness

The typical vertical distributions of skewness for longitudinal components of velocity in the main channel (verticals 37–39) are shown in Fig. 5. Near the bottom its values are close to zero, and at $z/h = 0.4$ it reaches the lowest negative value equal to -0.5. Further, together with the increase of z/h until the level $z/h = 0.6$, the skewness increases to zero and then till $z/h = 0.8$ the skewness remains almost constant. The values of skewness for flow over the inclined wall (verticals 34–36) start from almost zero near the bed and next they decrease to -0.5 at $z/h = 0.2$–0.4 and above this level they remain negative. The skewness calculated for lateral component of turbulent velocity v is very small and close to zero in the main channel and it is relatively small and positive above the left inclined wall and the opposite above the right wall.

5.3. Kurtosis

The vertical distributions of kurtosis of longitudinal turbulent velocities in the main channel (verticals 37–39) and above the inclined wall (verticals 32–36) are presented

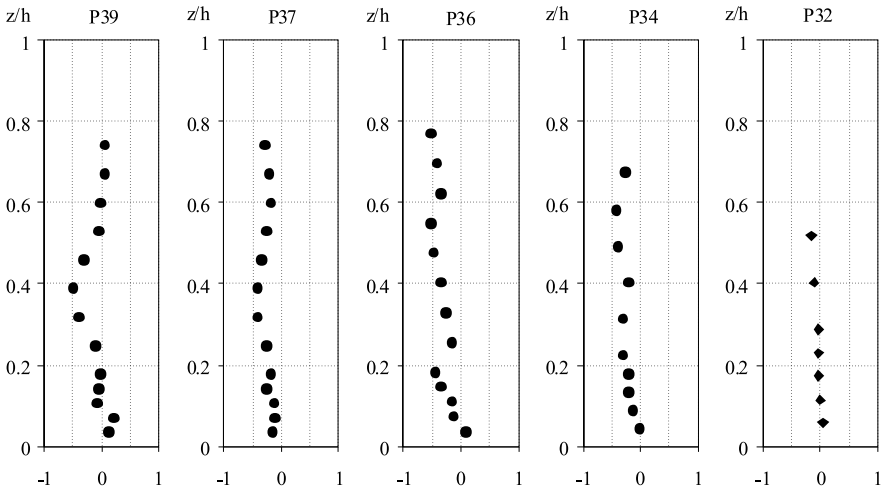

Fig. 5. Vertical distribution of the longitudinal component of the skewness coefficient in the main channel (verticals 37–39) and above the inclined wall (verticals 32–36)

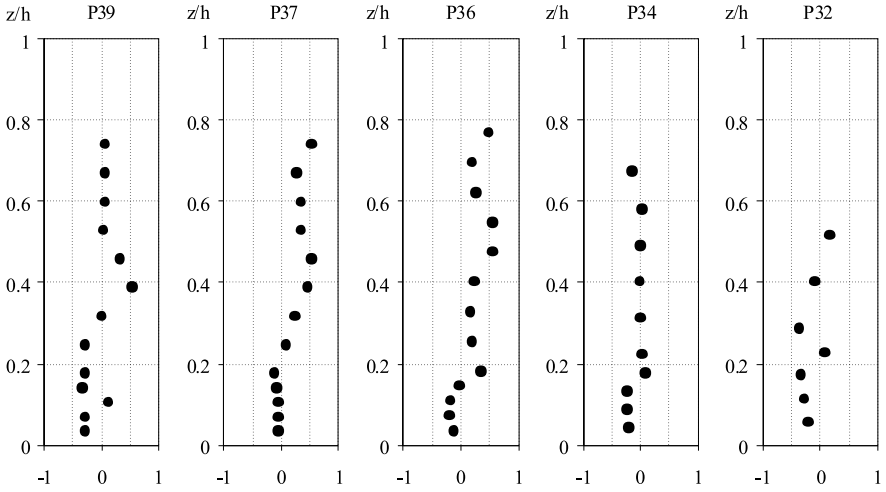

Fig. 6. The vertical distribution of kurtosis of the longitudinal velocity in the main channel (verticals 37–39) and above the inclined wall (vertical 32–36)

in Fig. 6. In the main channel, the kurtosis increases from the negative values near the bottom ($z/h < 0.3$) to its maximum values equal to +0.5 at the level $z/h = 0.4$, and it again decreases to zero at the level of about $z/h = 0.6$ for vertical 39 and 0.2 for vertical 37 (see Fig. 6). Values of kurtosis for the interactive zone are scattered and it is difficult to find any regularity. The kurtosis of other components

of turbulent velocities are distributed along the depth similar to the longitudinal ones, but their values in the vertical direction are larger than in the lateral direction.

5.4. Reynolds Stresses

Turbulent shear stresses τ_{zx} in the main channel (Fig. 7, verticals 37–39) linearly decrease from relatively large values close to the channel bed to the zero value at the level ca. $z/h = 0.7$. They remain constant until the level $z/h = 0.8$ where last measurements were made. Those trivial values of turbulent shear stresses result from the two-stage geometry of the cross-section causing the generation of additional non-vanishing stresses caused by secondary currents counterbalancing the stresses due to gravity (Eq. 2). At the same time one may observe almost zero values of shear stresses τ_{yx} in the main channel (Fig. 8). The vertical variations of shear stresses τ_{zx} above the inclined walls are rather chaotic, the fact that might be explained by studying Eq. (2). Due to that equation, the disturbances in linear changes of the stresses above the sloping banks are caused by non-vanishing variations of τ_{yx} as well as non-zero secondary currents. It seems, however, that the influence of those secondary currents is somewhat lower as was suggested by Knight, Shiono (1990). Fig. 7 presents the variations of the shear stresses τ_{zx} above the sloping banks – those stresses vanish at various levels, namely at the level $z/h = 0.5$ at the vertical 36 and close to the water surface at the vertical 32. It means that the influence of the inclination of the channel wall decreases together with the increase in distance from the channel axis.

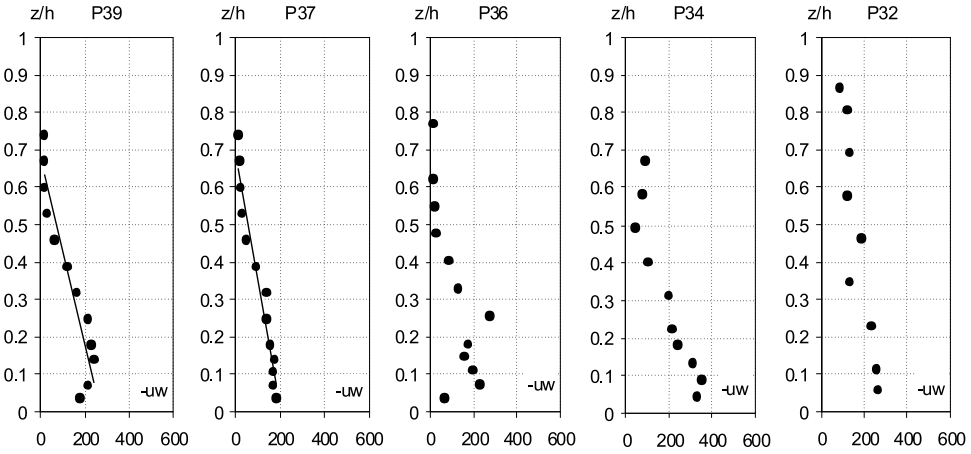

Fig. 7. Vertical distribution of the Reynolds stresses (τ_{zx}/ρ), in the main channel (H = 0.283 m)

The lateral variation of the Reynolds stresses τ_{yx} at given elevation, z, above the local bed is shown in Fig. 8. The stresses τ_{yx} near the channel centerline are

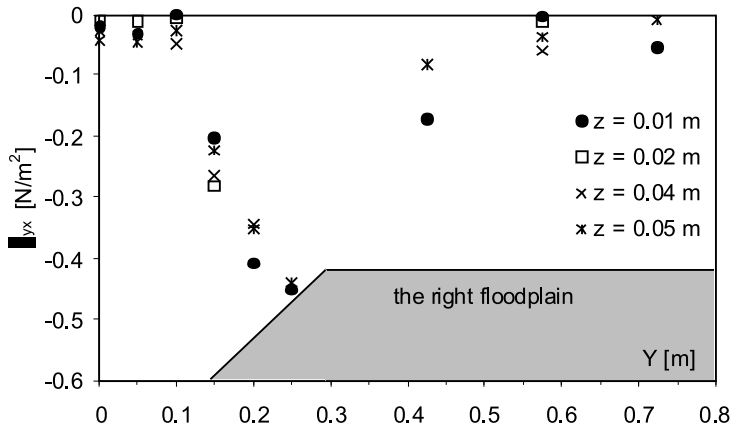

Fig. 8. Lateral distribution of the Reynolds stress, τ_{yx}, at different levels and water depth $H = 0.283$ m

close to zero, and as the distance from the centerline increases, these stresses also increase. The maximum stresses occur close to the beginning of the floodplain (see Fig. 8). Such result has also been obtained by Arnold and Rouve (1989) and Knight and Shiono (1990).

6. Autocorrelation, Scales and Spectral Density Function

The form of autocorrelation functions of the longitudinal velocities is similar at each measuring point; it starts from unity for $t = 0$, then its values decrease and from a certain point they oscillate in an irregular way close to zero. Typical graphs of $r_E(t)$ can easily be found in literature (e.g. Nezu and Nakagawa 1993). The maximum values of Eulerian integral time scale, T_E, defined by Eq. (10) and calculated for the channel centerline, range from 0.3 s till 0.7 s. Taking into account the Taylor hypothesis of "frozen turbulence" the evaluated normalized integral scales L/h are in the range from 0.2 to 1. The vertical profiles of the Eulerian integral length scale normalized by the local depth for main channel are displayed in Fig. 9. It is obvious that those scales grow from the lowest values at the points close to the bed to their maximum values at water surface.

The energy or power density spectrum $E(f)$, defined by Eq. (11), for three different distances from the bed ($z = 1$ cm, 15 cm and 19 cm) at the vertical located in the channel centerline are presented in Fig. 10. The calculated spectrum may have a very large variance so that the spectrum has very large oscillations. To decrease the variance, the frequency smoothing is usually applied using spectral windows. In this paper, the Tukey window is used. This window has a weighting function for the averaging that is a cosine function with a half wavelength equal to the width of the window and with the maximum weighting being at the center of the

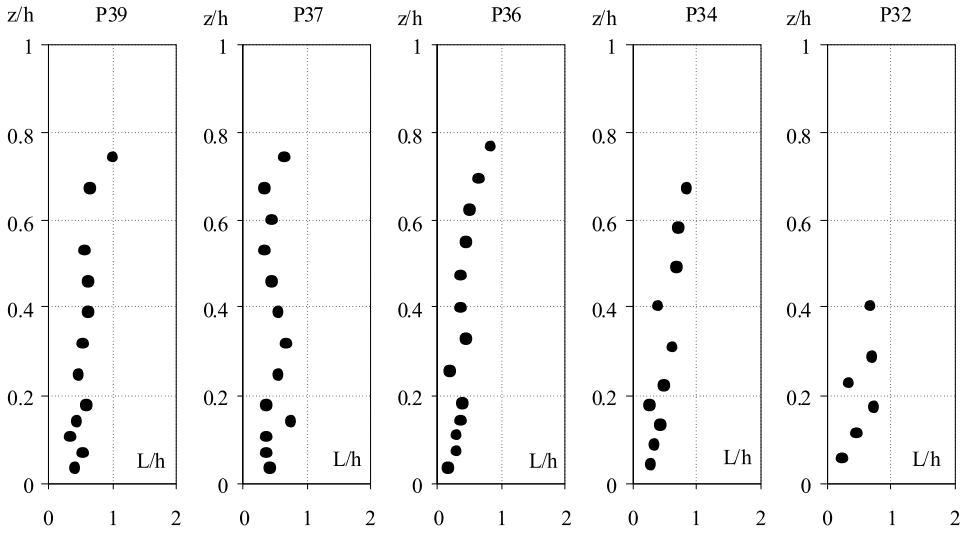

Fig. 9. Eulerian integral longitudinal length scale in the main channel

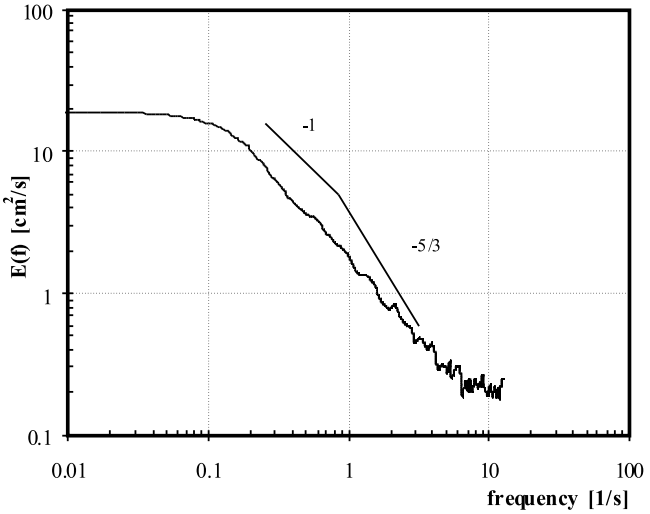

Fig. 10. Spectral distribution in channel centerline at z = 1 cm

window. The width of the window was chosen by trial and error method to be 7 seconds and it allowed to minimize the fluctuations in the spectra without loosing the essential aspects of the shape of the spectral distributions. In our analysis, the relative shape of the spectrum was more important than the actual values, since only the shape was needed to identify the Kolmogorov inertial subrange and other frequency subranges.

Some other researchers (see for example Nikora 1999) analyze additionally a subrange of frequencies where the spectrum decays as $G(f) \sim f^{-1}$. It happens in shear flows without solid boundaries and this subrange is situated in the equilibrium range of frequencies close to the energy-containing eddies. It may be assumed that in this subrange the energy dissipation is expressed as $\varepsilon(k) \sim u_*^3 k$, where k is the longitudinal wave number in the direction of the mean flow, where homogeneity applies.

The inertial subrange within which "–5/3 power law" applies as well as "–1" subrange of frequencies are detected in the channel centerline (see Figures 10–12). At the distance 1 cm from the channel bottom the inertial subrange is located at frequencies from 0.9 Hz to 3 Hz, at 15 cm from the bottom in the range from 0.65 Hz to 1.5 Hz, and at 19 cm it ranges from 0.55 Hz to 1.2 Hz. It is easy to see that the inertial subrange begins at 0.9 Hz at the point 1 cm from the bed and for larger distances from the bed that subrange begins at lower frequencies. For localization of the "–1" subrange see Figures 10–12. These figures show that this subrange becomes shorter as the distance from the bed increases.

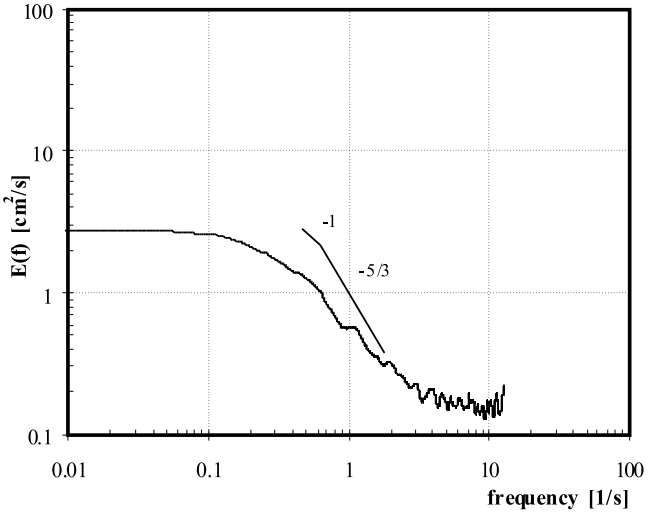

Fig. 11. Spectral distribution in channel centerline at z = 15 cm

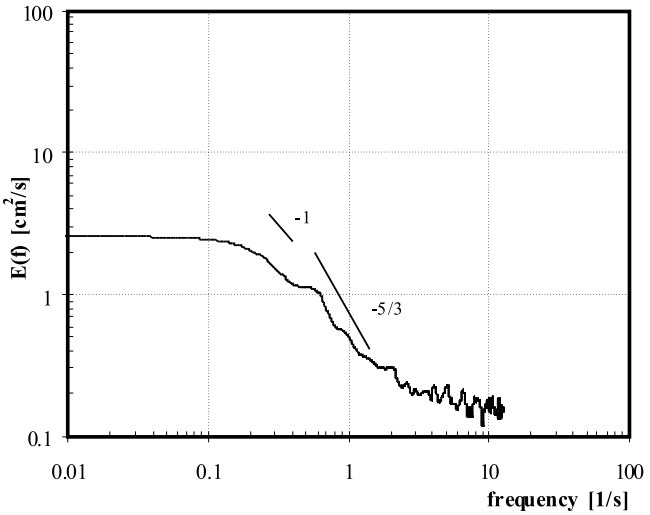

Fig. 12. Spectral distribution in channel centerline at z = 19 cm

When analyzing the above figures it is possible to identify the characteristic scale of large horizontal motion playing an important role in mixing and dispersion in shallow water flows (see Prooijen, Uijttewall 2005). This motion reaches about 1 m at the distance of 19 cm above the channel bed (it is seen at $f = 0.4$ s^{-1}), and the size about 0.4 m (corresponding to frequency 1 Hz) at 15 cm above the channel bed (the mean velocity for these two distances are about 0.4 m/s). Also, it is possible to find out some details of this motion, analyzing the smoothing spectra with narrow windows, of the 5 s or less.

7. Conclusions

The following conclusions may be drawn from the measurements of instantaneous velocities in steady turbulent flow in two-stage trapezoidal channel.

1. The vertical distributions of primary velocity are generally logarithmic in the main channel, where the lateral shear stresses τ_{yx}, as well as the transversal components of mean velocities are low.
2. The vertical distributions of turbulent intensity follow standard, exponential form in the main channel. The appropriate empirical coefficients deviate from those for 2D uniform flow, because the inclined wall affects the intensities. The ratios between the longitudinal, lateral and vertical intensities for the channel centerline are 2.3 : 1.5 : 1.0, respectively.
3. The spatial distributions of primary velocity, turbulent intensity and Reynolds stresses over the inclined rough wall are different from those in the main channel.

Primary velocities almost follow the logarithmic law, but with universal constant B much lower than in the main channel. The wall suppresses the turbulent intensities and they vary from the lowest values at the vertical 36 (the corner between the main channel and inclined wall) to the highest ones at the vertical 32. The vertical distributions of Reynolds stresses, τ_{zx}, over the inclined wall are definitely not linear. Reynolds stresses τ_{yx} assume the largest values close to the corner between the main channel and the floodplain.

4. The values of skewness and kurtosis clearly indicate deviation from Gaussian distribution of fluctuating, longitudinal velocities. The vertical distributions of skewness and kurtosis coefficients show that the skewness in the main channel (verticals 39 and 37) reaches the lowest negative value equal to -0.5 at $z/h = 0.4$. On the contrary, the kurtosis for the main channel takes its largest positive values at $z/h = 0.4$. The skewness calculated for lateral component of turbulent velocity is very small and close to zero in the main channel and it is relatively small above the inclined walls.
5. Eulerian integral length scale for the main channel grows from the lowest values at points close to the bed to its maximum value at the water surface.
6. The inertial subrange of energy density spectrum for the main channel is detected in the channel centerline. Left border of the inertial subrange, i.e., the lowest frequency of this subrange, increases from the water surface towards the channel bed. The band of frequencies for inertial subrange is rather wide near the bed and becomes narrower when approaching the water surface.

Acknowledgements

This paper is the result of a collaborative work for which funding was provided by two grants of the Polish Ministry of Science and Higher Education – Grant No. 2 P04D 026 29 and 2 P06S 028 29.

References

Arnold U. (1989) Turbulence and Mixing Mechanisms in Compound Open Channel Flow, *23rd Congress IAHR*, Ottawa, Canada, 1–8.

Arnold U., Rouve G. (1989) A Review of Investigations on Compound Open-Channel, In: *Proc. Hydrocomp'89*, Dubrovnik, Yugoslavia, 1–22.

Babaeyan-Koopaei K., Ervine D. A., Carling P. A., Cao Z. (2002) Velocity and Turbulence Measurements for Two Overbank Flow Events in River Severn, *Journal of Hydraulic Engineering,* **128** (10), 891–900.

Buffin-Bélanger T., Roy A. G. (2005) 1 min in the life of a river: selecting the optimal record length for the measurement of turbulence in fluvial boundary layers, *Geomorphology*, **68**, 77–94.

Czernuszenko W., Rylov A. (2002) A turbulence model for trapezoidal channels, In: Zech Y., Bousmar D. (eds.), *River Flow*, Balkema, Leiden, 75–81.

Hinze J. O. (1975) *Turbulence*, McGraw-Hill Book Company, New York.

Knight D. W. (1989) River Flow Simulation: Research and Developments, *Journal of the Institution of Water and Environmental Managment,* **4** (2), 163–175.

Knight D. W., Shiono K. (1990) Turbulence measurements in a shear layer region of a compound channel, *Journal of Hydraulic Research*, **28** (2), 175–195.

Knight D. W., Shiono K. (1996) River Channel and Floodplain Hydraulics, In: Anderson, Walling, Bates (eds.), *Floodplain Processes*, J. Wiley, 139–181.

Knight D. W., Yuen K. W., Alhamid A. A. (1994) Boundary Shear Stress Distribution in open channel flow, In: Bevea K., Chatwin R., Millbank J. (eds.), *Physical Mechanics of Mixing and Transport in the Environmental*, J. Wiley, 1–38.

Lohrmann A., Cabrera R., Kraus N. (1994) Acoustic-Doppler Velocimeter (ADV) for Laboratory Use, *Fundamentals and Advacements in Hydraulic Measurements and Experimentation*; *Proc.*, Buffalo, New York, 351–365.

Naot D., Nezu I. (1993) Hydrodynamic Behavior of Compound Rectangular Open Channels, *Journal of Hydraulic Engineering,* **119**, 390–408.

Nezu I., Nakagawa H. (1993) *Turbulence in Open-Channel Flows*, Balkema, Rotterdam.

Nezu I., Onitsuka K., Sagara Y., Iketani K. (1999) Secondary currents and bed shear stress in compound open-channel flows with shallow flood plain, *XXVIII Congress IAHR*.

Nikora V. (1999) Origin of the "-1" spectral law in wall-bounded turbulence, *Physical Review Letters*, **83** (4), 734–736.

Prooijen B. C., Uijttewaal W. S. J. (2005) Horizontal mixing in shallow flows, In: Czernuszenko W., Rowiński P. M. (eds.), *Water Quality Hazards and Dispersion of Pollutants*, Springer.

Rhodes D. G., Knight D. W. (1994) Velocity and boundary shear in a wide compound duct, *Journal of Hydraulic Research*, **32** (5), 743–764.

Rowiński P. M., Czernuszenko W., Kozioł A. P., Kubrak J. (2002) Properties of a streamwise turbulent flow field in an open two-stage channel, *Archives of Hydro-Engineering and Environmental Mechanics*, **49** (2), 37–57.

Rowiński P. M., Mazurczyk A. (2006) Turbulent characteristics of flows through emergent vegetation, In: Ferreira R. M. L., Alves E. C. T. L., Leal J. G. A. B., Cardoso A. H. (eds.), *River Flow*, Taylor & Francis Group, London, 623–630.

Shiono K., Knight D. W. (1990) Mathematical Models of Flow in Two or Multi Stage Straight Channels, *International Conference on River Flood Hydraulics*, 229–238.

Shiono K., Knight D. W. (1991) Turbulent open-channel flows with variable depth across the channel, *J. Fluid Mech.*, **222** (7), 617–646.

Tominaga A., Ezaki K., Nezu I., Nakagawa H. (1989), Three-dimensional turbulent structure in straight open channel flows, *Journal of Hydraulic Research,* **27**, 149–173.